Understanding trends in lithium binding at two-dimensional materials

Srdjan Stavrić, Zoran S. Popović, and Željko Šljivančanin*
Vinča Institute of Nuclear Sciences, University of Belgrade, P.O. Box 522, RS-11001 Belgrade, Serbia

(Received 6 July 2018; revised manuscript received 29 October 2018; published 26 November 2018)

Layered structure and peculiar electronic properties of two-dimensional (2D) materials foster the concept of utilizing them as main components of lithium-ion batteries. Understanding basic physical mechanisms governing the interaction of Li with 2D crystals is of key importance to succeeding in a rational design of cathode and anode materials with superior functionalities. In this study density functional theory was applied to reveal the microscopic picture of Li interaction with 15 2D crystals, including several transition metal oxides and dichalcogenides, carbides of Group XIV elements, functionalized graphene, silicene, and germanene, as well as black phosphorus and Ti_2C MXene. We found that the general trend in Li binding can be estimated from positions of conduction band minima of 2D materials, since the energy of the lowest empty electronic states shows a nice correlation with the strength of Li adsorption. At variance to the majority of studied surfaces where the electron transferred from Li is spread across the substrate, in monolayers of carbides of Group XIV elements the interaction with Li and the charge transfer are well localized. This gives rise to their capability to accommodate Li structures with a nearly constant binding energy of alkaline atoms over Li coverages ranging from well-separated adatoms to a full monolayer.

DOI: 10.1103/PhysRevMaterials.2.114007

I. INTRODUCTION

Comprehensive research efforts, triggered by the isolation and characterization of a single graphene layer [1], have generated a whole new class of two-dimensional (2D) materials with diverse structural and electronic properties [2–5]. Further advances in designing artificial materials have been achieved by assembling 2D crystals into van der Waals (vdW) heterostructures. This opens prospects to tailor properties of heterostructures by the choice of the stacking sequence of 2D building blocks [6]. 2D materials and their vdW heterostructures are promising candidates for key components of several future technologies, for example, post-silicon transistors [7,8], next generation of solar cells [9], or advanced Li ion batteries (LIB) [10,11]. The efficiency of LIB, the main energy storage systems currently utilized in portable electronic devices or electrical cars, relies on materials with the ability to adsorb and quickly transport large quantities of lithium. These functionalities are governed by the strength of Li binding as well as mobility of adsorbed atoms.

Due to their relevance to LIB technologies, combined with the interest in understanding microscopic mechanisms guiding Li interaction with 2D materials, the number of studies focused on fundamental properties of these systems is rapidly growing. Paticularly well studied is Li adsorption at graphene [12–14]. Density functional theory (DFT) studies confirmed pronounce charge transfer from the adsorbate to the surface as expected for the element with very low electronegativity. This is accompanied by a strong repulsive interaction between positively charged Li adatoms. The same effect is found in DFT investigations of alkaline metal atoms attached to other 2D crystals. Ab initio studies included Li adsorption at MXenes [15], black phosphorus (BP) [16–18], SiC [19], MoO_2 [20], MnS_2 monolayer [21], and $MnO_{2(1-x)}Se_{2x}$ monolayer [22]. Recently, DFT was also applied to investigate Li binding to MoS_2 [23,24] monolayer, MXenes/graphene heterostructures [25], and graphene/MoS_2 bilayers [26] or composites [27].

Initial steps in a rational design of advanced LIB with electrodes based on vdW heterostructures rely on understanding microscopic mechanisms governing Li adsorption and mobility at 2D materials, utilized as the building blocks in their vertical heterostructures. To shed light on these details we applied DFT, a methodology able to provide an accurate picture of structural and electronic properties of Li adsorbates at 2D materials. We found that general trends in Li binding at these surfaces can be rationalized based on their basic electronic properties, namely the energies of the lowest unoccupied electronic states. Carbides of Group XIV elements and graphane show distinct behavior compared to other studied 2D crystals since the key role in Li binding is played by new electronic states, emerged on these surfaces upon Li adsorption.

The manuscript is organized as follows: In Sec. II we describe computational methodology applied in this work; Sec. III presents results on structural properties and binding energies of Li adsorbates at examined 2D crystals, combined with the discussion on observed trends. The main results are summarized in Sec. IV.

II. COMPUTATIONAL DETAILS

DFT calculations were carried out using GPAW code [28], based on the real-space projector augmented waves (PAW) method [29,30], where wave functions were represented on a real space grid with the spacing of 0.15 Å. Li atom adsorption

*zeljko@vinca.rs

on 2D crystals was modeled using a 4×4 rhombohedral cell containing 16 atoms per atomic layer (transition metal oxides and dichalcogenides) or 16 atoms per sublattice of the honeycomb structure (carbides of Group XIV elements, hydrogenated or fluorinated graphene, silicane, and germanane). The same simulation cells were used to calculate adsorption geometries and binding energies of Li dimers at CrO_2 and SnC monolayers. Test calculations performed for Li atom adsorption on SnC and CrO_2 monolayers show that the choice of the 4×4 surface unit cell provides well-converged binding energies at computational cost considerably smaller compared to larger surface unit cell sizes (see Table S1 of the Supplemental Material [31]). The studies of high coverage Li structures at these two surfaces were performed within a smaller surface unit cells, described in Sec. III B. In the calculations of Li adatom at black phosphorous, the surface was represented by a rectangular cell with 36 phosphorus atoms. For all investigated surfaces we carried out the calculations with theoretically optimized lattice constants. In addition to this, the periodic boundary conditions were imposed in the plane of 2D materials, while in the direction perpendicular to the surface were used open boundary conditions, with at least 8 Å of vacuum on each side of the surface. The geometry optimization was performed by means of Broyden-Fletcher-Goldfarb-Shanno algorithm [32] assuming that the equilibrium structure was found when the maximal atomic forces were smaller than 0.05 eV/Å. The convergence criteria during the self-consistency cycle are as follows: the energy between last three consecutive iterations changes less than 0.5 meV, the change in integrated absolute value of electron density is less than 0.0001 electrons per valence electron and the integrated value of the square of the residuals of the Kohn-Sham equations is less than 1.0×10^{-6} eV^2 per valence electron. The surface Brillouin zone sampling was done according to the Monkhorst-Pack scheme [33], with 16 **k**-points. The conduction band minima of pristine surfaces were calculated with 1×1 surface cells and using at least 256 Monkhorst-Pack **k**-points. The effects of electronic exchange and correlation were taken into account by means of Perdew-Burke-Ernzerhof (PBE) parametrization form within generalized gradient approximation. The electronic states of nonmagnetic structures were occupied according to Fermi-Dirac distribution corresponding to the temperature of 0.1 eV. The temperature of Fermi-Dirac distribution used in the calculations of magnetic Li structures at 2D materials was lowered to 0.03 eV. The electrons of atoms present in studied structures, considered as valence, are listed in Table S2 of the Supplemental Material [31].

III. RESULTS AND DISCUSSION

We applied DFT to examine trends in Li binding at selected 2D crystals, starting with adsorption of individual Li atoms. Due to the periodic boundary conditions used in the calculations, Li adatoms form ordered structures with the coverage Θ smaller than 0.1 monolayers (ML). The list of studied 2D materials includes transition metal dichalcogenide monolayers (MoS_2, $MoSe_2$, CrS_2 and $CrSe_2$), transition metal oxide monolayers (MoO_2 and CrO_2), MXene (Ti_2C monolayer), Group XIV carbide monolayers (SiC, GeC and SnC), hydrogenated silicine (Si-H), germanine (Ge-H) and graphene (Gra-H), black phosphorus (BP), as well as fluorinated graphene (Gra-F). The selection of 2D structures made in this work was motivated by efforts to study structurally different 2D materials which carry out distinct electronic properties. Also, we selected 2D materials with different chemical reactivity in order to inspect surfaces with a large variation in the binding energy of Li adatoms. From low Li coverage studies, we identified two classes of 2D materials featuring qualitatively different interaction with lithium. Then we used SnC and CrO_2 monolayers as representatives of these two families of 2D crystals, and examined favorable structures formed at them by densely packed Li adsorbates. For metal oxides, dichalcogenides, and MXenes, the coverage of 1 ML corresponds to structures where the number of Li and metal atoms is equal. Regarding 2D materials with honeycomb lattice the coverage is defined as a ratio between the number of Li adatoms and available sublattice sites. The results for hexagonal boron nitride (h-BN) were not included in the present study since from test calculations we found that Li does not bind to it.

TABLE I. Binding energies of Li atom at 2D materials together with the position of their conduction band minimum (CBM) and midgap states. All energies are in eV.

	2D crystal	CBM	Midgap state	Li binding energy (E_B)
1	Graphane (Gra-H)	−1.30	−2.87	0.01
2	SiC	−2.51	−3.91	1.00
3	GeC	−2.75	−4.21	1.43
4	Silicane (Si-H)	−2.87	–	0.64
5	SnC	−3.56	−4.19	1.88
6	Germanane (Ge-H)	−3.71	–	0.93
7	$MoSe_2$	−3.89	–	1.43
8	Black phosphorus (BP)	−4.17	–	1.98
9	MoS_2	−4.25	–	1.79
10	Fluoronated graphene (Gra-F)	−4.48	–	1.78
11	Ti_2C	−4.52	–	2.31
12	$CrSe_2$	−4.57	–	2.06
13	CrS_2	−4.98	–	2.45
14	MoO_2	−5.79	–	2.99
15	CrO_2	−6.99	–	4.23

A. Low Li coverage

DFT calculations reveal that Li adsorption geometries at 15 2D crystals listed in Table I can be categorized into six different groups, presented in Fig. 1. Figure 1(a) depicts the most favorable binding site of Li adatom at hydrogenated monolayers of C, Si, and Ge, known as graphane, silicane, germanane, as well as at fully fluorinated graphene. At each of these surfaces Li binds in the threefold hollow site next to three H or F atoms.

The second group of monolayers with a very similar binding geometry of Li adatoms includes SiC, GeC and SnC [Fig. 1(b)], where Li also binds in the threefold hollow site

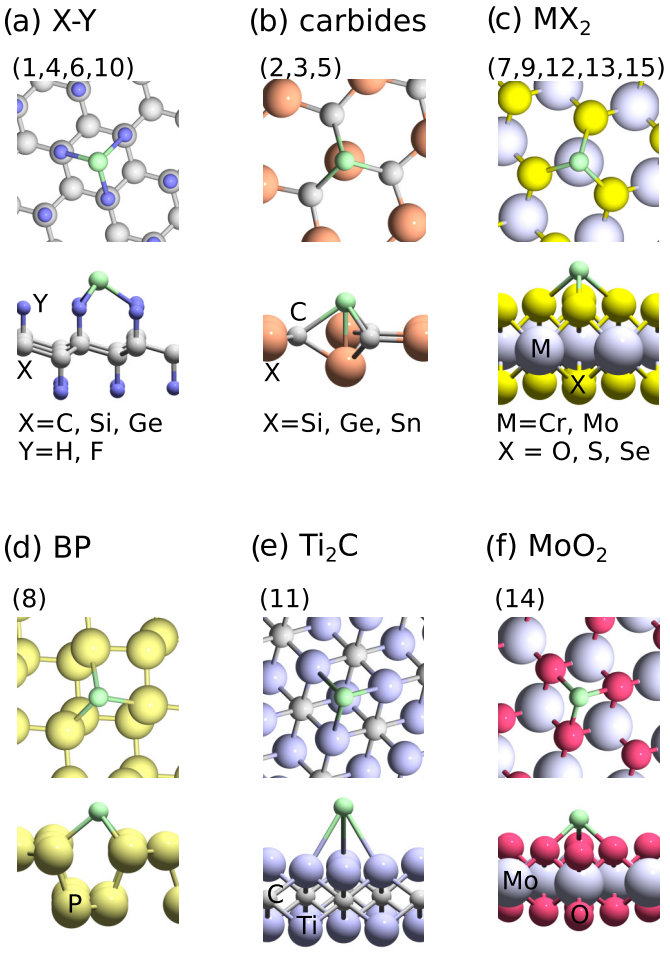

FIG. 1. Top and side views of Li adatom at 2D crystals, classified into the groups with qualitatively the same adsorption geometries: (a) graphane, silicane, germanane or fluorinated graphene; (b) SiC, GeC and SnC monolayers; (c) MX_2 monolayers; (d) black phosphorus; (e) Ti_2C; and (f) MoO_2 monolayer. Li atoms are presented as small green spheres; the numbers correspond to the enumeration of 2D structures in Table I.

between C atoms, atop a Group XIV element (Si, Ge, or Sn), which is markedly displaced from the atomic surface plane. Different types of threefold hollow sites are preferred Li binding geometries at MX_2 monolayers [Fig. 1(c)], at BP and at Ti_2C monolayers, as shown in Figs. 1(d) and 1(e), respectively. In contrast to other MX_2 layers, listed in Fig. 1(c), the most favorable Li binding site at MoO_2 is a threefold hollow site without metal atom underneath [Fig. 1(f)]. The details on lattice constants of all fifteen 2D crystals, Li atom adsorption geometries, and the Li distance to the nearest atoms on the surface are presented in Table S3 of the Supplemental Material [31]. Due to low electronegativity, shared by all alkaline metals, Li adatoms show strong tendency to transfer the 2*s* electron to the surface they are adsorbed at. At semiconducting or insulating surfaces the electron is transferred to the states near the conduction band minimum (CBM), representing the lowest empty states in the system. Hence, it is likely to expect a correlation between the energy gain due to charge transfer from Li adatom to the

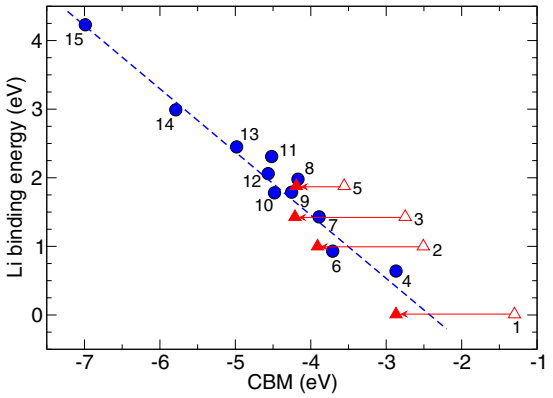

FIG. 2. Correlation between Li atom binding energy (E_B) and conduction band minimum (CBM) for selected 2D crystals; surfaces without and with midgap state, induced upon Li adsorption, are marked with blue circles and red rectangles, respectively. Arrows indicate energy shifts from CBM to the energies of midgap states. The numbering of 2D materials is the same as in Table I. The dashed line serves as a guide to eyes.

surface and the position of the CBM. Since the energy gain can be quantified as Li binding energy (E_B), we plotted E_B as a function of CBM for fifteen 2D materials considered in this work, as shown in Fig. 2. The plot indeed demonstrates a strong correlation between Li binding energy and the position of CBM of pristine 2D crystals. The highest E_B of 4.23 eV was calculated for Li adatoms at CrO_2. This 2D material features the lowest energy of the CBM of nearly −7 eV below the vacuum level, in a sharp contrast with graphane (fully hydrogenated graphene) where the CBM is only 1.3 eV below vacuum. The high energy of graphane's CBM is accompanied with the Li binding energy of only 0.01 eV. For other 2D materials the values of E_B and CBM are between these two limits (Table I). Ti_2C is the only metal among studied 2D crystals, and instead of CBM, the position of the lowest empty states is determined by Fermi level.

Among studied 2D materials we chose CrO_2 as the one with the strongest interaction with Li, and in Fig. 3(a) plotted density of states (DOS) of CrO_2 monolayer with adsorbed Li atom. For the sake of completeness we also plotted DOS of a pristine monolayer. Figure 3(a) demonstrates that Li adsorbate donates 2*s* electron to the conduction band of CrO_2 and shifts Fermi level of a clean monolayer by 0.44 eV. Apart from the change in the occupation, CrO_2 electronic states near CBM are barely affected by Li adsorbate. This is further confirmed by the plot of DOS projected on 2*s* orbital of Li adatom. The peak in Fig. 3(b) is located nearly 1 eV above Fermi level, and Li-2*s* DOS at energies near CBM is negligible. The states at the top of valence and at the bottom of conduction band are predominantly of Cr-3*d* character and there is a small contribution from O-2*p* orbitals. Li-2*s* electron, transferred to lower part of the conduction band of the monolayer has been delocalized across the sheet, as shown in the plot of electron density induced upon Li interaction with CrO_2 [Fig. 4(a)]. The effect of Li adatom on electronic properties of several other 2D materials are presented in Fig. S1 of the Supplemental Material [31]. It shows the total DOS of pristine surfaces,

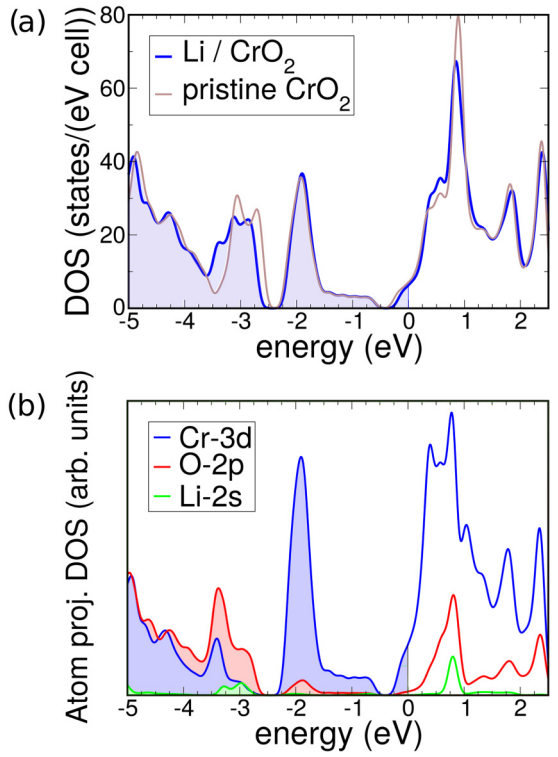

FIG. 3. (a) Total DOS of pristine CrO_2 monolayer and the monolayer with adsorbed Li atom; (b) DOS od the CrO_2 monolayer with adsorbed Li atom, projected on relevant atomic orbitals.

as well as DOS of these surfaces with added Li atom. In Figs. S1a and S1b are presented total DOS of BP and silicane, typical examples of 2D crystals where Li adsorption is accompanied by a charge transfer, without any substantial

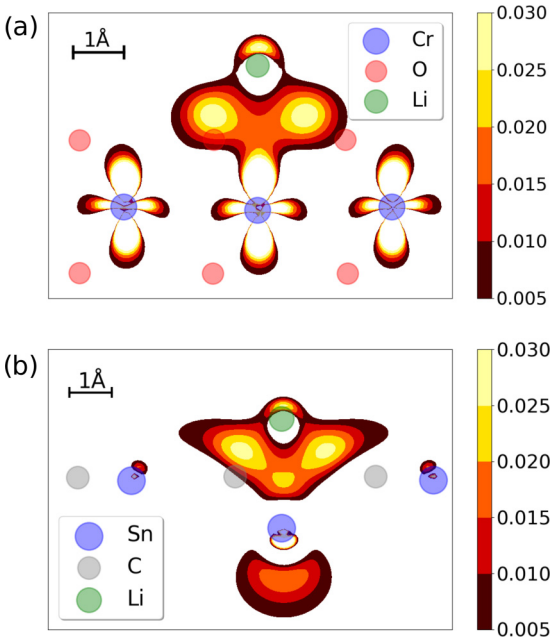

FIG. 4. Electron density induced upon Li adsorption at (a) CrO_2 and (b) SnC monolayer; only isocontours corresponding to charge accumulation are plotted.

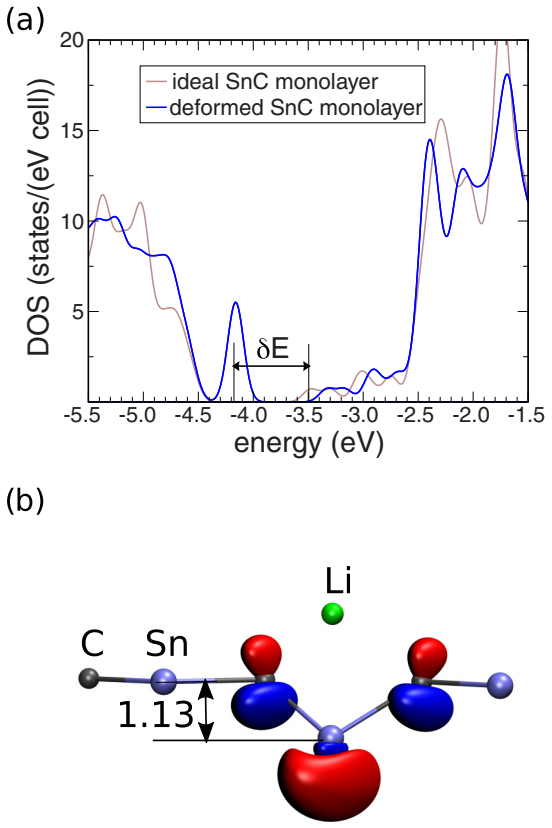

FIG. 5. (a) Total DOS of pristine SnC monolayer calculated for the ideal sheet (brown curve) and deformed monolayer (blue line) where Sn and C atoms are fixed at the positions as in SnC with Li adatom. δE indicates the position of the midgap state relative to the conduction band minimum (CBM) of ideal SnC monolayer; (b) Isosurface plot of Kohn-Sham wavefunction of the midgap state at Γ point. Regions with different signs of the wave function are colored differently. The number indicates displacement (in Å) of Sn from the plane of other Sn atoms, induced by Li adsorbate.

changes in the structural properties of the surfaces. Figures S1d and S1e present total DOS of SiC and GeC with and without Li adatoms. The results are common to 2D structures with midgap states induced by Li adatom.

At variance with the most of studied structures, where the calculated points in Fig. 2 are aligned along the dashed line, the results for SnC, GeC, SiC, and graphane show a pronounced deviation from it. To emphasize these differences the corresponding points in Fig. 2 are marked as open red triangles. Closer inspection reveals that after adsorption of Li atom, midgap states appear on each of these four surfaces. The corrections to the correlation plot, obtained by taking into account that the lowest empty states at these surfaces are actually midgap states, are presented as filled triangles in Fig. 2. The horizontal, arrowed lines indicate energy shifts from the CBM of ideal surfaces to the energies of corresponding midgap states. For all three carbide monolayers Li adsorption is accompanied with a significant surface deformation. Si, Ge, or Sn atom underneath Li adsorbates are pulled inward, which triggers the formation of midgap states [Fig. 5(a)], located at displaced atoms. Li-2*s* electron is transferred to

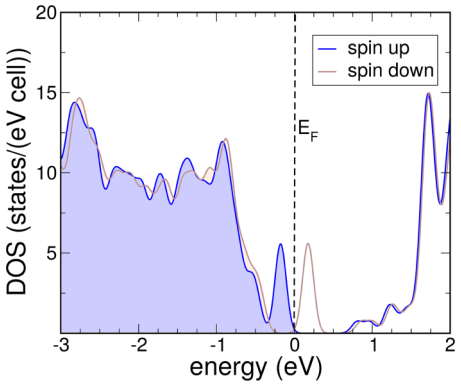

FIG. 6. Total DOS of SnC monolayer with adsorbed Li atom.

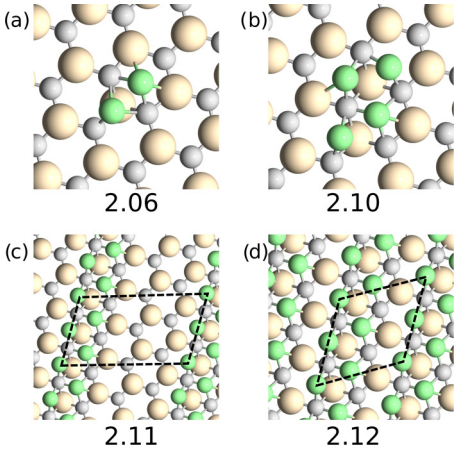

FIG. 7. Atomic structure of (a) Li dimer, (b) Li tetramers and the most stable ordered structures on SnC monolayer at Li coverage, (c) $\Theta = 1/2$ ML, and (d) $\Theta = 1$ ML. Sn, C, and Li atoms are represented by large yellowish, small gray, and green spheres, respectively. The numbers indicate Li binding energy in eV per atom. A full monolayer (ML) represents the coverage where the number of Li and Sn atoms is equal. Surface unit cells of ordered structures are marked with black dashed lines.

midgap states, and their highly localized character favors spin polarization. Similar effects were recently reported in the studies of Li adsorption at SiC monolayer [19,34]. Adsorbate-induced structural deformation of all three monolayers is well correlated to the strength of Li binding. In Fig. 5(b) is shown the effect of Li adsorbate on displacements of atoms in SnC monolayer, with emphasize on the Sn atom which is dislocated by as much as 1.13 Å from its position in pristine SnC. The corresponding values for Si and Ge atoms in their carbide monolayers were 0.75 and 0.90 Å, respectively. The isosurface plot of the Kohn-Sham wave function is presented in Fig. 5(b). Li adatoms induce spin polarization of each of three studied carbide monolayers with the total magnetic moment of 1 μ_B. Total DOS of Li atom on SnC monolayer, depicted in Fig. 6 clearly demonstrates that only spin up midgap state is occupied. The plot of charge density induced at SnC upon Li adsorption verifies that the Li-2s electron is transferred to the midgap state mainly localized at Li adatom, with a small contribution from few surface atoms nearby it [Fig. 4(b)]. This is markedly different from the corresponding plot of the charge transfered from Li to CrO_2 monolayer [Fig. 4(a)] and fully in the line with qualitatively different nature of Li binding at these two types of 2D materials.

In contrast to their interaction with monolayers of Group XIV carbides, Li atoms weakly bind to graphane, and the surface deformation induced by the adsorbate is negligible. The induced midgap state and spin polarization are mainly localized at Li adatom. One unpaired electron gives rise to the total magnetic moment of 1 μ_B.

B. High Li coverage

For applications of 2D crystals as components of cathode or anode electrodes in LIB, of particular relevance is their ability to accommodate densely packed Li adsorbates. From the study of low coverage Li structures, described in Sec. III A, we identified two classes of 2D materials carrying out qualitatively different interaction with isolated Li adatoms. We now examine high coverage Li structures formed at (i) SnC monolayer, representing a sheet where the interaction of Li adatoms with the surfaces is well localized, and (ii) CrO_2 monolayer, a typical example of a 2D material where the interaction with Li is fairly delocalized.

As an initial step in the investigation of high Li coverage structures at 2D materials we chose to investigate the interaction between two Li atoms, adsorbed closely to each other. In Fig. 7(a) are depicted DFT results of calculated atomic structure and binding energy of Li dimer at SnC monolayer. The binding energy of 2.06 eV per atom is larger than 1.88 found for isolated Li adatom on the same surface, indicating an attractive interaction between Li adsorbates. The stability of adsorbed Li dimers originates from the midgap state. It emerges upon adsorption of a single Li atom but can accommodate two electrons (see Fig. 6). Therefore when two Li adatoms are adsorbed next to each other, in the structure presented in Fig. 7(a), two Li-2s electrons are transferred to the midgap state. At variance to the adsorption of two well separated Li atoms, where the cost of the deformation of the SnC layer caused by adsorbates adds, for Li dimer this energy penalty is shared by two Li atoms. Total DOS and DOS projected on 2p atomic orbitals of Sn and C atoms in vicinity of Li adsorbates confirm that the midgap state is fully occupied [Figs. 8(a) and 8(b)]. Changes in the Li binding per atom, found in tetramer [Fig. 7(b)] and high Li coverage structures in Figs. 7(c) and 7(d), are small compared to the binding of an isolated Li dimer in Fig. 7(a). In all of these adsorption structures the number of Li adatoms is twice the number of created midgap states. The broadening of the peak in DOS of the Li monolayer on SnC, presented in Figs. 8(c) and 8(d), is due to hybridization of the midgap states located on neighboring Sn atoms. Adsorption of individual Li atoms triggers local spin-polarization of SnC layer due to the occupation of only one spin channel of the midgap state. The adsorption structures with Li dimers are nonmagnetic.

Li dimer structure at CrO_2 monolayer is depicted in Fig. 9(a). The black crosses in the figure indicate initial positions of Li atoms, placed above nearby Cr atoms. Yet, a strong repulsion between them increases Li-Li distance as

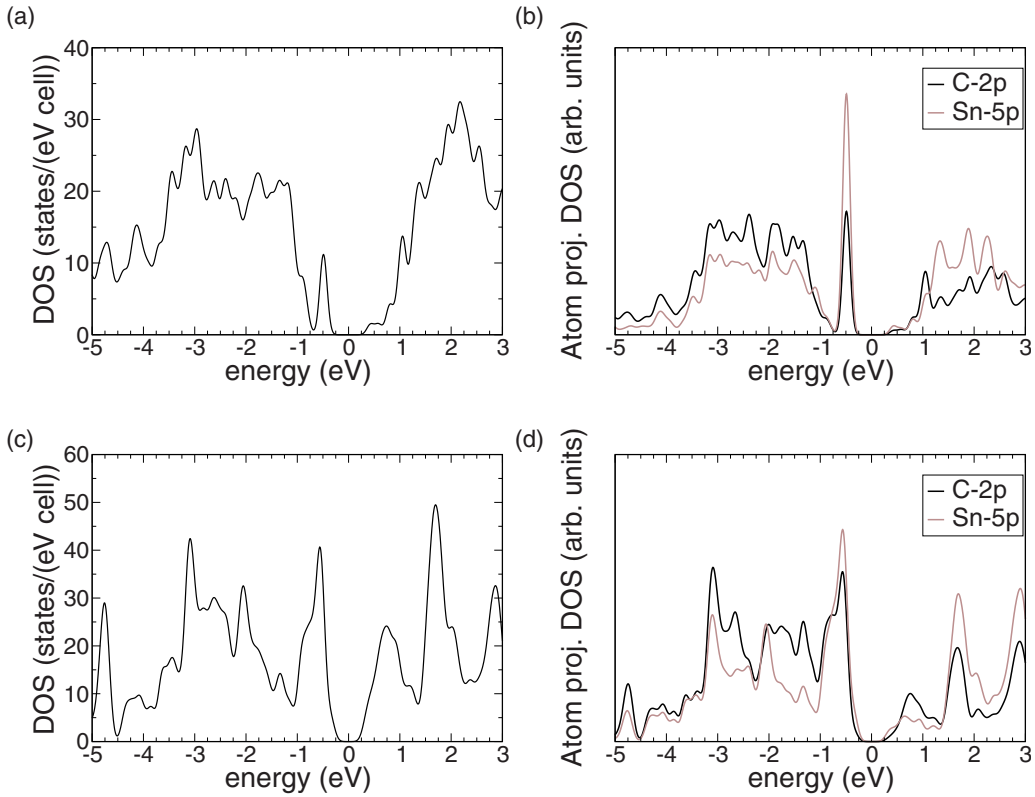

FIG. 8. Total and Atom projected DOS of (a), (b) Li_2 dimer and (c), (d) Li monolayer on SnC.

marked by the arrows, and the stable dimer structure is one in Fig. 9(a). The Li binding energy of 4.00 eV per atom is 0.23 eV smaller compared to the one of an isolated Li adatom at the same surface. Thus, Li adatoms on CrO_2 do not show tendency towards clustering. The ordered Li structures on CrO_2 monolayer, as well as the corresponding binding energies for coverages Θ of 1/4, 1/3 and 1/2 ML are given in Fig. 9(b)–9(d), respectively.

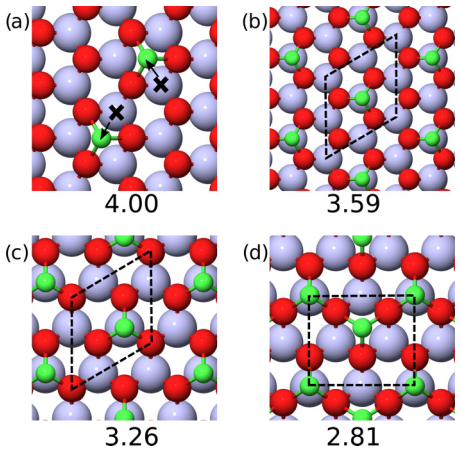

FIG. 9. Atomic structure of (a) Li dimer and the most stable ordered structures at CrO_2 monolayer at Li coverage, (b) $\Theta = 1/4$ ML, (c) $\Theta = 1/3$ ML, and (d) $\Theta = 1/2$ ML. The numbers indicate Li binding energy in eV per atom; Cr, O, and Li atoms are represented by light blue, red, and green spheres, respectively. A full monolayer (ML) refers to the coverage where the number of Li and Cr atoms are equal. Surface unit cells are marked with black dashed lines.

In contrast to SnC where we found a very weak variation of the binding with Li coverage once Li_2 are formed, Li binding at CrO_2 monolayer shows a monotonic decrease with an increase in Li coverage Θ, reaching the value of 2.81 eV per atom at $\Theta = 0.5$ ML. This is as much as $\sim$1.5 eV less than the binding of an isolated Li atom on the same sheet. An increase of Li coverage at CrO_2 monolayer gives rise to the unfavorable accumulation of electrons in the conduction band of the pristine monolayer, and thus weakens lithium binding.

The effect of Li adsorbates on structural properties of these materials, in particular, the lattice constant variation with Li coverage, is highly relevant for their applications as electrodes in Li-ion batteries. To examine the volume expansion effect in lithiated 2D materials we considered CrO_2 and SnC monolayers with Li coverage of 1/2 and 1 ML, respectively, and calculated their equilibrium lattice constants. For CrO_2 we found the lattice constant increase of 2% compared to the pristine layer. At variance to this the lattice constant decreases 1% in lithiated SnC relative to pristine sheet. However, Li adsorption causes corrugation of the SnC layer and the average metal-metal distance in high Li coverage structure of SnC is actually 2% larger than in the pristine SnC. These calculations indicate modest changes in the lattice constants of lithiated 2D materials, which should not significantly degradate their structural stability.

An additional interesting effect studied in SnC and CrO_2 monolayers is the evolution of the work function with Li coverage. For SnC and CrO_2 we assumed Li adsorption geometries in Figs. 1(b) and 1(c) and performed calculations

TABLE II. Evolution of SnC and CrO_2 monolayer work functions with Li coverage. For both surfaces the calculations were performed using rhombohedral unit cells of different sizes. All energies are in eV.

Coverage (ML)	SnC	CrO_2
0	4.54	7.33
1/16	4.07	5.28
1/9	3.84	4.11
1/4	3.18	1.40

within rombohedral surface unit cells with sizes in the range from 4×4 to 2×2. The results presented in Table II show that at both surfaces work function decreases with an increase in Li coverage. The work function of CrO_2 decreases from 7.33 eV to only 1.40 eV when Li coverage changes from 0 to 1/4 ML. The corresponding change of work function of SnC is from 4.54 to 3.18 eV. The shift in Fermi levels closer to vacuum level partially contributes to this. However, on the CrO_2 a dipole layer, emerged between positively charged Li ions and negatively charged surface, creates a strong electric field which considerably reduces the work function. The strength of the field rapidly increases with the Li coverage. The effect on SnC sheet is less pronounced due to different Li adsorption geometry and localized character of the charge transfer.

IV. CONCLUSIONS

Using DFT calculations we examined Li binding at fifteen different 2D crystals which are considered as promising candidates for application as the building blocks of the novel cathode and anode materials in LIB. The expectation that at low coverage Li binding to 2D crystals causes only minor changes in their structural properties and the effect of the adsorbate on electronic properties of the surfaces is limited to a simple charge transfer, was confirmed for the majority of studied 2D structures. Yet, much more complicated Li binding picture, involving considerable structural deformation and qualitative changes in electronic properties of 2D crystals, was found for four of investigated layers—graphane, SiC, GeC, and SnC. Employing the position of the conduction band minimum (CBM) of studied surfaces as a single parameter describing their electronic properties, for the majority of considered 2D materials we found an excellent correlation between CBM and Li atom binding energy. Discrepancy observed for carbides of Group XIV elements and graphane was explained in terms of midgap states emerged at these surfaces upon Li adsorption. Due to localized nature of the interaction between Li and the surfaces with midgap states, they are able to preserve the nearly constant value of Li binding energy for adsorbates varying from isolated dimers to ordered structures with Li coverage of 1 ML. From DFT studies we identify SnC as particularly promising 2D crystal for applications as the electrodes of Li-ion batteries, since it shows high structural stability, together with a modest variation in Li binding energy and the lattice constant over a wide range of Li coverage. These results indicate that sheets of SnC combined in multilayers or vdW heterostructures with 2D materials like graphene could be utilized as building blocks of materials able to easily store and release a large amount of Li. However, the energetics of Li binding in multilayers of 2D materials is different from the binding on single layers [14,26] and further studies are needed to confirm this.

ACKNOWLEDGMENTS

This work has been supported by the Serbian Ministry of Education and Science under Grant No. ON171033, by the Qatar National Research Fund (a member of the Qatar Foundation) through the NPRP Grant No. 7-665-1-125, and by the COST Action MP1402-HERALD. The calculations were performed at the PARADOX-IV supercomputer at the SCL of the Institute of Physics Belgrade supported by Grant No. ON171017 and at RAAD2 supercomputer of Texas A&M University at Qatar.

[1] A. K. Geim and K. S. Novoselov, Nat. Mater **6**, 183 (2006).
[2] S. Z. Butler, S. M. Hollen, L. Y. Cao, Y. Cui, J. A. Gupta, H. R. Gutierrez, T. F. Heinz, S. S. Hong, J. X. Huang, A. F. Ismach, E. Johnston-Halperin, M. Kuno, V. V. Plashnitsa, R. D. Robinson, R. S. Ruoff, S. Salahuddin, J. Shan, L. Shi, M. G. Spencer, M. Terrones, W. Windl, and J. E. Goldberger, ACS Nano **7**, 2898 (2013).
[3] S. Lebegue and O. Eriksson, Phys. Rev. B **79**, 115409 (2009).
[4] H. Sahin, S. Cahangirov, M. Topsakal, E. Bekaroglu, E. Akturk, R. T. Senger, and S. Ciraci, Phys. Rev. B **80**, 155453 (2009).
[5] F. A. Rasmussen and K. S. Thygesen, J. Phys. Chem. C **119**, 13169 (2015).
[6] A. K. Geim and I. V. Grigorieva, Nature **499**, 419 (2013).
[7] X. B. Li, J. X. Wu, N. N. Mao, J. Zhang, Z. B. Lei, Z. H. Liu, and H. Xu, Carbon **92**, 126 (2015).
[8] B. Radisavljevic, A. Radenovic, J. Brivio, V. Giacometti, and A. Kis, Nat. Nanotechnol. **6**, 147 (2011).
[9] W. J. Yu, Y. Liu, H. L. Zhou, A. X. Yin, Z. Li, Y. Huang, and X. F. Duan, Nat. Nanotechnol. **8**, 952 (2013).
[10] K. Chang, W. X. Chen, L. Ma, H. Li, H. Li, F. H. Huang, Z. Xu, Q. B. Zhang, and J. Y. Lee, J. Mater. Chem. **21**, 6251 (2011).
[11] Q. L. Sun, Y. Dai, Y. D. Ma, T. Jing, W. Wei, and B. B. Huang, J. Phys. Chem. Lett. **7**, 937 (2016).
[12] K. T. Chan, J. B. Neaton, and M. L. Cohen, Phys. Rev. B **77**, 235430 (2008).
[13] A. M. Garay-Tapia, A. H. Romero, and V. Barone, J. Chem. Theory Comput. **8**, 1064 (2012).
[14] S. Stavrić, M. Belić, and Ž. Šljivančanin, Carbon **96**, 216 (2016).
[15] Y. Xie, M. Naguib, V. N. Mochalin, M. W. Barsoum, Y. Gogotsi, X. Q. Yu, K. W. Nam, X. Q. Yang, A. I. Kolesnikov, and P. R. C. Kent, J. Am. Chem. Soc. **136**, 6385 (2014).
[16] Q. F. Li, C. G. Duan, X. G. Wan, and J. L. Kuo, J. Phys. Chem. C **119**, 8662 (2015).

[17] T. Hu and J. Hong, J. Phys. Chem. C **119**, 8199 (2015).
[18] Y. Ding and Y. Wang, J. Phys. Chem. C **119**, 10610 (2015).
[19] R. J. Baierle, C. J. Rupp, and J. Anversa, Appl. Surf. Sci. **435**, 338 (2018).
[20] Y. Zhou and C. Geng, Nanotechnology **28**, 105402 (2017).
[21] C. C. Leong, H. Pan, and S. K. Hoa, Phys. Chem. Chem. Phys. **18**, 7527 (2016).
[22] F. Ersan, G. Gökoğlu, and E. Aktürk, J. Phys. Chem. C **119**, 28648 (2015).
[23] W. A. Saidi, Cryst. Growth Des. **15**, 3190 (2015).
[24] D. Nasr Esfahani, O. Leenaerts, H. Sahin, B. Partoens, and F. M. Peeters, J. Phys. Chem. C **119**, 10602 (2015).
[25] Y. Aierken, C. Sevik, O. Gülseren, F. M. Peeters, and D. Çakir, J. Mater. Chem. A **6**, 2337 (2018).
[26] Ž. Šljivančanin and M. Belić, Phys. Rev. Mater. **1**, 044003 (2017).
[27] X. J. Shao, K. D. Wang, R. Pang, and X. Q. Shi, J. Phys. Chem. C **119**, 25860 (2015).
[28] J. Enkovaara, C. Rostgaard, J. J. Mortensen, J. Chen, M. Dulak, L. Ferrighi, J. Gavnholt, C. Glinsvad, V. Haikola, H. A. Hansen, H. H. Kristoffersen, M. Kuisma, A. H. Larsen, L. Lehtovaara, M. Ljungberg, O. Lopez-Acevedo, P. G. Moses, J. Ojanen, T. Olsen, V. Petzold, N. A. Romero, J. Stausholm-Moller, M. Strange, G. A. Tritsaris, M. Vanin, M. Walter, B. Hammer, H. Hakkinen, G. K. H. Madsen, R. M. Nieminen, J. K. Norskov, M. Puska, T. T. Rantala, J. Schiotz, K. S. Thygesen, and K. W. Jacobsen, J. Phys. Condens. Matter **22**, 253202 (2010).
[29] P. E. Blöchl, Phys. Rev. B **50**, 17953 (1994).
[30] J. J. Mortensen, L. B. Hansen, and K. W. Jacobsen, Phys. Rev. B **71**, 035109 (2005).
[31] See Supplemental Material at http://link.aps.org/supplemental/10.1103/PhysRevMaterials.2.114007 for total DOS of BP, silicane, SiC, and GeC monolayers with and without Li adatom. Variation of Li binding energies on SnC and CrO_2 with the size of the unit cell, the list of valence electrons of relevant atoms and data on structural properties of Li adatoms on studied 2D materials are provided in Tables S1–S3.
[32] D. C. Liu and J. Nocedal, Math. Program. **45**, 503 (1989).
[33] H. J. Monkhorst and J. D. Pack, Phys. Rev. B **13**, 5188 (1976).
[34] M. Luo, H. H. Yin, and Y. H. Shen, J. Supercond. Nov. Magn. **31**, 1235 (2018).